

Modeling carbon to nitrogen and carbon to chlorophyll *a* ratios in the ocean at low latitudes: Evaluation of the role of physiological plasticity

*Nathalie Lefèvre*¹

Department of Biological Sciences, University of Essex, Colchester CO4 3SQ, Great Britain; Plymouth Marine Laboratory, Prospect Place, West Hoe, Plymouth PL1 3DH, Great Britain

Arnold H. Taylor and Francis J. Gilbert

Plymouth Marine Laboratory, Prospect Place, West Hoe, Plymouth PL1 3DH, Great Britain

Richard J. Geider

Department of Biological Sciences, University of Essex, Colchester CO4 3SQ, Great Britain

Abstract

Simulation modeling provides a means for testing the limits of our quantitative understanding of the factors that control phytoplankton biomass, growth rate, and primary productivity in the sea. We simulated the annual cycles of chlorophyll *a* (Chl *a*) concentration, primary productivity, nitrogen export, phytoplankton carbon to nitrogen (C:N) and carbon to Chl *a* ratios (C:Chl *a*) using a physiological model of phytoplankton carbon, nitrogen, and Chl *a* dynamics. The model was embedded within a one-dimensional physical model of vertical exchanges that included simple mortality and recycling terms. A sensitivity analysis allowed evaluation of the relative effects of changes in phytoplankton physiology, physical forcing, mortality, and nutrient cycling on Chl *a* distributions and phytoplankton C:N. Critical to the success of the model was the treatment of mortality, which included seasonal (temperature) and depth-related components, and the treatment of recycling efficiency, which was considered to be a function of the inorganic nitrogen concentration. The subtropical simulation compared favorably with data obtained at the Bermuda Atlantic Time-series Study (BATS) station. Our results illustrate the utility of physiological data in validation of biogeochemical models. In particular, model predictions of phytoplankton C:Chl *a*, which ranged from 30 to 170 g C (g Chl *a*)⁻¹, compared well with direct estimates based on ¹⁴C labeling of Chl *a*. However, predictions of phytoplankton C:N, which ranged from ~5–9 g C (g N)⁻¹, could not be verified because of lack of data. This range of C:N suggests a slight limitation of phytoplankton growth rates by nutrients in surface waters.

At the heart of pelagic biogeochemical models are the phytoplankton because they are responsible for carbon dioxide fixation. In addition, the extensive and growing database of chlorophyll *a* (Chl *a*) measurements provides the major reality check on the performance of pelagic biogeochemical models. Despite the explicit treatment of phytoplankton growth in these models, growth rates generated by the models typically do not agree with observations. Observed phytoplankton growth rates (μ) in the mixed layer of subtropical gyres typically equal 0.6–0.7 d⁻¹ (Lessard and Murrell 1998; Claustre et al. 1999; Stelfox-Widdicombe et al. 2000), whereas models typically return values of 0.1–0.2 d⁻¹ (Fasham et al. 1990; Doney et al. 1996). Observations indicate that the phytoplankton relative growth rate (μ/μ_m) is not severely nutrient-limited in subtropical and tropical

regions ($\mu/\mu_m > 0.7$) (Taguchi et al. 1988; Laws et al. 1989; Allen et al. 1996), whereas models typically indicate otherwise ($\mu/\mu_m \approx 0.1$) (Fasham et al. 1990; Doney et al. 1996). The inability of most models to generate realistic phytoplankton growth rates or realistic estimates of the degree of nutrient limitation has not been widely recognized, but raises concern about the general applicability of these models.

The performance of pelagic ecosystem models has usually been evaluated in terms of the ability to account for seasonal cycles of Chl *a*, inorganic nitrogen concentrations, and primary productivity. Despite the increasing complexity of pelagic biogeochemical models in terms of phytoplankton physiology and differentiation of phytoplankton functional groups (Moore et al. 2001), the implications of the models for phytoplankton growth rate and physiology have rarely been examined. As noted above, biogeochemical models often fail to reproduce what we know about the relative growth rate of phytoplankton in the oligotrophic ocean. Confidence in our ability to quantitatively model plankton ecosystems will be enhanced if models can also be validated against physiological variables. Verifying that biogeochemical models can provide accurate information on phytoplankton carbon to Chl *a* (C:Chl *a*) and carbon to nitrogen (C:N) ratios will enhance our ability to translate pigment fields into biomass fields and link pelagic carbon and nitrogen cycles. A model that includes phytoplankton physiology must not only reproduce the seasonal and depth dependencies of biomass

¹ To whom correspondence should be addressed. Present address: School of Environmental Sciences, University of East Anglia, Norwich NR4 7TJ, Great Britain.

Acknowledgments

We gratefully acknowledge the Bermuda Biological Station for Research, Inc., and the U.S. National Science Foundation for provision of the data from the Bermuda Atlantic Time-series Study (BATS) station, which has proven to be such an important resource for our work. This research was supported by the U.K. Natural Environment Research Council through grant NER/B/S/1999/00022.

(i.e., Chl *a*) and primary productivity (i.e., ^{14}C assimilation) but should also reproduce the seasonal and depth dependencies of phytoplankton C:N and phytoplankton C:Chl *a*, as well as growth rate (μ) and relative growth rate (μ/μ_m).

In this paper, we employ a simple ecological model that includes only phytoplankton and inorganic nitrogen in simulations of phytoplankton dynamics in subtropical and tropical systems. Our treatment of phytoplankton physiology is more sophisticated than in most models and accounts for the dynamics of organic carbon, organic nitrogen, and Chl *a* (Geider et al. 1998). This treatment of the phytoplankton has already been incorporated into an intermediate complexity model by Moore et al. (2001), who extended the Geider et al. (1998) model to include iron, phosphorous, and silicate limitation. However, Moore and coworkers did not discuss the physiological implications of the model. Furthermore, Moore et al. (2001) applied the model only to the wind-mixed layer; as such, they did not consider the vertical structure of the water column and, in particular, the development and maintenance of the Chl *a*-maximum layer.

We employed the Geider et al. (1998) physiological model within a simple ecological model with prescribed physics. As in many other models of upper ocean biogeochemistry, we specified the seasonal cycles of the depth and temperature of the mixed layer and employed a fixed eddy diffusivity (k) to account for vertical exchange below the mixed layer. Phytoplankton death and the consequent recycling and export of nitrogen were treated in terms of a mortality coefficient (m) and a recycling coefficient (ε). By fixing a coefficient for the mortality, there is no need to differentiate between losses to grazing, viruses, or spontaneous death. This has the advantage of minimizing the number of variables in the model. Mortality has been found to be depth dependent (Liu et al. 1997), and our mortality coefficient was prescribed to vary both seasonally and with depth, whereas the recycling coefficient was made a function of the inorganic nitrogen concentration. We show that the model can reproduce the seasonal and vertical distributions of Chl *a*, the seasonal cycle of primary productivity, and the seasonal and depth dependencies of phytoplankton C:Chl *a* as well as generate a narrow range of phytoplankton C:N and hence a narrow range of relative growth rates.

Methods

Model structure—We employed a one-dimensional water column model based on Taylor et al. (1997) to describe the seasonal variations of the vertical distributions of phytoplankton carbon (C), phytoplankton nitrogen (PN), Chl *a*, and a single nutrient (total inorganic nitrogen designated N) over an annual cycle at 0 and 30°N latitude. These variables were calculated as a function of depth and time.

$$\frac{\partial C}{\partial t} = P^c C - mC - \zeta V^c C - R^c C + \frac{\partial}{\partial z} \left[k \frac{\partial C}{\partial z} \right] \quad (1)$$

$$\begin{aligned} \frac{\partial \text{Chl } a}{\partial t} &= \rho_{\text{chl}} V^c C - m \text{Chl } a - R^{\text{chl}} \text{Chl } a \\ &+ \frac{\partial}{\partial z} \left[k \frac{\partial \text{Chl } a}{\partial z} \right] \end{aligned} \quad (2)$$

$$\frac{\partial \text{PN}}{\partial t} = V^c C - m \text{PN} - R^{\text{PN}} \text{PN} + \frac{\partial}{\partial z} \left[k \frac{\partial \text{PN}}{\partial z} \right] \quad (3)$$

$$\frac{\partial N}{\partial t} = -V^c C + \varepsilon m \text{PN} + R^{\text{PN}} \text{PN} + \frac{\partial}{\partial z} \left[k \frac{\partial N}{\partial z} \right] \quad (4)$$

P^c is the carbon-specific photosynthesis rate, V^c is the carbon-specific nitrogen assimilation rate, ρ_{chl} is the ratio of Chl *a* synthesis to nitrogen assimilation, and ζ is the cost of nitrogen assimilation. The phytoplankton are subject to losses from phytoplankton respiration (R^c , R^{chl} , and R^{PN}) or mortality (m), which regenerates nutrients with efficiency ε . Phytoplankton are assumed to be neutrally buoyant within a hydrodynamic regime defined by a turbulent diffusion coefficient k . Each variable was defined on a vertical grid of 40 points with a spacing of 5 m. The differential equations (Eqs. 1–4) were approximated by finite-difference equations using the Crank–Nicholson scheme as in Taylor et al. (1997).

Physical forcing—The model was forced by prescribed physics. The incident radiation at the sea surface, the temperature of the mixed layer, and the mixed-layer depth all vary seasonally in the model according to Taylor et al. (1991). The irradiance at the sea surface depends on the peak daily irradiance (I_{max}) and the number of hours of daylight (H_d), which were calculated as in Sellers (1965). The light intensity at the sea surface was then calculated for any time of day (t_d) from Eq. 5.

$$I_{\text{surf}} = I_{\text{max}} [(H_d - 12)/H_d + 12 \sin(t_d/12)/H_d] \quad (5)$$

The temperature in the mixed layer was represented by a sine wave fitted to the climatology of Levitus and Boyer (1994).

$$\begin{aligned} T &= T_{\text{min}} + 0.5(T_{\text{max}} - T_{\text{min}}) \\ &\times \{1 + \sin[2\pi(D - 135.5)/365]\} \end{aligned} \quad (6)$$

T_{max} and T_{min} are the maximum and minimum temperatures over the year, and D is the day (1 January being day 1). The depth of the mixed layer was modeled as described by Taylor et al. (1991). We adopted the same seasonal pattern of variation of mixed layer depth as Sarmiento et al. (1989), scaled with the minimum and maximum depths of the mixed layer from Levitus and Boyer (1994). Mixed layer depth for tropical regions was set to 30 m. Mixed layer depth for the subtropical simulation ranged from 25 m in summer to 125 m in spring.

The vertical mixing was parameterized by a turbulent diffusion coefficient, k , as in Taylor et al. (1997). The coefficient in the mixed layer was varied for the different runs (see Tables 1, 2). Beneath the mixed layer, a value of $7 \times 10^{-5} \text{ m}^2 \text{ s}^{-1}$ was used. Once a day, the mixed layer was homogenized to simulate diurnal convective mixing.

Light attenuation—When calculating light penetration down the water column, the surface light was divided equally into red and blue-green bands that were assumed to decay exponentially.

$$I = 0.5 I_{\text{surf}} e^{-k_r z} + 0.5 I_{\text{surf}} e^{-k_g z} \quad (7)$$

Table 1. Parameters of the model and typical values (see figure and table legends for variations that were applied for particular model runs).

Variable	Definition of the variable	Value	Units
m	Mortality	0.8	d^{-1}
k	Diffusion coefficient	0.0001	$m^2 s^{-1}$
α_{chl}	Chlorophyll-specific light absorption coefficient	7.5×10^{-6}	$g C m^2 (g Chl a (\mu mol photons)^{-1})^{-1}$
ζ	Cost of nitrogen assimilation	2	$g C (g N)^{-1}$
h	Mixed layer depth at the equator	30	m
E_a	Activation energy	70000	$J mol^{-1}$
K_N	Half-saturation constant of Monod equation	0.1	$\mu mol L^{-1}$
T_{ref}	Reference temperature	293	K
P_{max}^C	Maximum photosynthesis rate at T_{ref}	2.0	d^{-1}
θ_m^N	Maximum Chl a : nitrogen ratio	2.0	$g Chl a (g N)^{-1}$
R	Universal gas constant	8.3	$J mol^{-1} K^{-1}$
V_{max}^C	Maximum value of V^C	0.63	$g N (g C)^{-1} d^{-1}$
R_{ref}	Degradation rate constant at T_{ref}	0.1	d^{-1}

I_{surf} is the light intensity at the sea surface, $k_r = 0.4 + 0.04[Chl a]^{0.7}$ is the extinction coefficient for the red light, and $k_g = 0.02 + 0.08[Chl a]^{0.7}$ is the extinction coefficient for the green light. The values of the coefficients are based on Morel (1988).

Phytoplankton growth rate—We employed a physiological model that accounts for acclimation of growth rate (μ), photosynthesis (P^C), respiration (R^C), C:Chl a , and the N:C (Q) of phytoplankton to irradiance (I), inorganic nitrogen concentration (N), and temperature (T) (Geider et al. 1998). Phytoplankton growth rate is not treated explicitly. Rather, growth arises from the interaction of carbon and nitrogen assimilation. Accompanying growth is Chl a synthesis, which is linked to nitrogen assimilation through a regulatory term.

Photosynthetic carbon fixation is the product of the phytoplankton biomass (C) and the carbon-specific photosynthesis rate (P^C). P^C is a function of irradiance (I) and Chl a :C, designated θ , as follows (Geider et al. 1998).

$$P^C = P_m^C \left[1 - \exp\left(-\frac{\alpha_{chl} I \theta}{P_m^C}\right) \right] \quad (8)$$

α_{chl} is the initial slope of the photosynthesis–irradiance (P-I) curve normalized to Chl a , and P_m^C is the light-saturated rate of photosynthesis normalized to carbon. P_m^C is a multiplicative function of a Droop nutrient limitation function and an Arrhenius temperature dependence (Geider et al. 1998).

$$P_m^C = P_{max}^C \left[\frac{Q - Q_{min}}{Q_{max} - Q_{min}} \right] \exp\left[-\frac{E_a}{R} \left(\frac{1}{T} - \frac{1}{T_{ref}} \right) \right] \quad (9)$$

P_{max}^C is the value of P_m^C at the reference temperature of 293 K (T_{ref}) under nutrient-replete conditions, Q is the N:C of the phytoplankton, Q_{max} and Q_{min} are its upper and lower bounds, E_a/R is the slope of an Arrhenius plot, and T is absolute temperature (K).

The carbon-specific nitrogen assimilation rate, V^C , is a multiplicative function of an Arrhenius temperature dependence and Michaelis–Menten nutrient uptake kinetics with

regulation of the maximum uptake velocity by Q (Geider et al. 1998). It is given by Eq. 10.

$$V^C = V_{max}^C \left[\frac{Q_{max} - Q}{Q_{max} - Q_{min}} \right]^n \exp\left[-\frac{E_a}{R} \left(\frac{1}{T} - \frac{1}{T_{ref}} \right) \right] \left(\frac{N}{N + K_N} \right) \quad (10)$$

V_{max}^C is the upper limit to V^C , n is a shape factor (0.05), K_N is the half-saturation constant for nitrogen assimilation, and the other terms are as described previously.

Carbon-specific Chl a synthesis is determined by the rate of nitrogen assimilation and a regulatory term (Geider et al. 1998).

$$[1/C] dChl a/dt = \rho_{chl} V^C \quad (11)$$

ρ_{chl} is the regulatory term that is defined as in Eq. 12.

$$\rho_{chl} = \theta_m^N \left(\frac{P^C}{\alpha_{chl} I \theta} \right) \quad (12)$$

θ_m^N is the maximum Chl a :N observed in cells acclimated to extremely low light (Geider et al. 1998).

Phytoplankton respiration is treated as the sum of the maintenance metabolic rate and the cost of biosynthesis (Geider et al. 1998). The maintenance respiration (R^C), chlorophyll degradation (R^{chl}), and phytoplankton nitrogen remineralization (R^{PN}) rates are expressed as in Eq. 13.

$$R_{ref} \exp\left[-\frac{E_a}{R} \left(\frac{1}{T} - \frac{1}{T_{ref}} \right) \right] \quad (13)$$

R_{ref} is the degradation rate at T_{ref} , T is temperature, T_{ref} is a reference temperature of 293 K, and E_a/R is the slope of an Arrhenius plot. The cost of biosynthesis is assumed to be proportional to the nitrogen assimilation rate and is given by ζV^C in Eq. 1.

Mortality—Losses of carbon, nitrogen, and Chl a from the phytoplankton pool by mortality (which includes grazing, among other loss processes) were treated as first-order processes (see Eqs. 1–4), as in Eq. 14.

Table 2. Surface values of phytoplankton carbon to nitrogen (C:N, g C [g N]⁻¹) and carbon to Chl *a* (C:Chl *a*, g C [g Chl *a*]⁻¹) ratios and phytoplankton nitrogen (PhyN, mmol m⁻³) for different sensitivity tests at day 281. The parameter values for the standard run are given in Table 1.

	Standard run	$P_{\max}^C = 1.5$	$P_{\max}^C = 2.5$	$\alpha_{\text{Chl}} = 0.50 \times 10^{-5}$	$\alpha_{\text{Chl}} = 1.50 \times 10^{-5}$	$Q_{\min} = 0.05$	$Q_{\min} = 0.06$	$k = 2 \times 10^{-4}$	$k = 0.5 \times 10^{-4}$
C:N	11.3	9.8	12.4	10.6	12.5	10.6	9.9	10.8	11.5
C:Chl <i>a</i>	95	91	98	75	138	93	90	83	102
PhyN	0.062	0.055	0.068	0.054	0.089	0.062	0.060	0.12	0.03

$$\frac{\partial X}{\partial t} = -mX \quad (14)$$

X is an index of phytoplankton biomass (i.e., C, PN, or Chl *a*) and m is the first-order mortality coefficient. For the tropical simulation, m was assumed to be a constant 0.8 d⁻¹ within the mixed layer and to decrease linearly with depth below the mixed layer to become 0.0 d⁻¹ at 120 m. This treatment is consistent with the observations of Liu et al. (1997) for mortality of *Prochlorococcus* in the subtropical North Pacific. For the subtropical simulations, m in the mixed layer was assumed to follow a sine wave that paralleled the seasonal cycle imposed on temperature to allow higher specific loss rates in summer (Taylor et al. 1991).

$$m = m_{\min} + 0.5(m_{\max} - m_{\min}) \times \{1 + \sin[2\pi(D - 135.75)/365]\} \quad (15)$$

The m_{\min} and m_{\max} are the minimum and maximum mortality values, and D is the day (1 January being day 1); m_{\min} was set to 0.3 d⁻¹ and m_{\max} to 0.8 d⁻¹. Below the mixed layer, m was assumed to decline linearly to 0.05 d⁻¹ at a depth of 120 m.

Nutrient cycling and export production—Phytoplankton mortality was assumed to regenerate nutrients with a recycling efficiency (ε) that was a function of the nutrient concentration, so that recycling became more efficient when nutrient was depleted (Eq. 16).

$$\varepsilon = 0.3 + \frac{(\varepsilon_{\max} - 0.3)K_N}{N + K_N} \quad (16)$$

ε_{\max} is the maximum recycling efficiency when N approaches zero ($N \ll K_N$). Thus, ε varies from 0.3 when $N \gg K_N$ to ε_{\max} when $N \ll K_N$. As in Taylor et al. (1997), we arbitrarily chose to scale the N dependence of recycling efficiency by K_N . Other scaling factors could have been employed to yield qualitatively similar results. Equation 16 incorporates the observation that the ratio of new to total production (f -ratio) is an asymptotic function of nitrate concentration (Platt and Harrison 1985). Nutrient that is not recycled is assumed to sink out of the euphotic zone immediately.

Export production was calculated as a sum of phytoplankton mortality and diffusion of nitrogen (Eq. 17).

$$(1 - \varepsilon)mPN + k \frac{\partial}{\partial z} PN \quad (17)$$

The diffusive flux was negligible compared to loss from phytoplankton mortality.

Results and discussion

Equatorial Atlantic simulations and sensitivity analysis—Initially, we examined the seasonal and vertical Chl *a* distributions for the equatorial simulation using the set of parameters listed in Table 1. The model was validated at the equatorial location near 25°W. The physics would have to be different to run it at another location. The simulated surface Chl *a* concentration did not vary significantly throughout the year, with concentrations ranging from 0.15 to 0.17

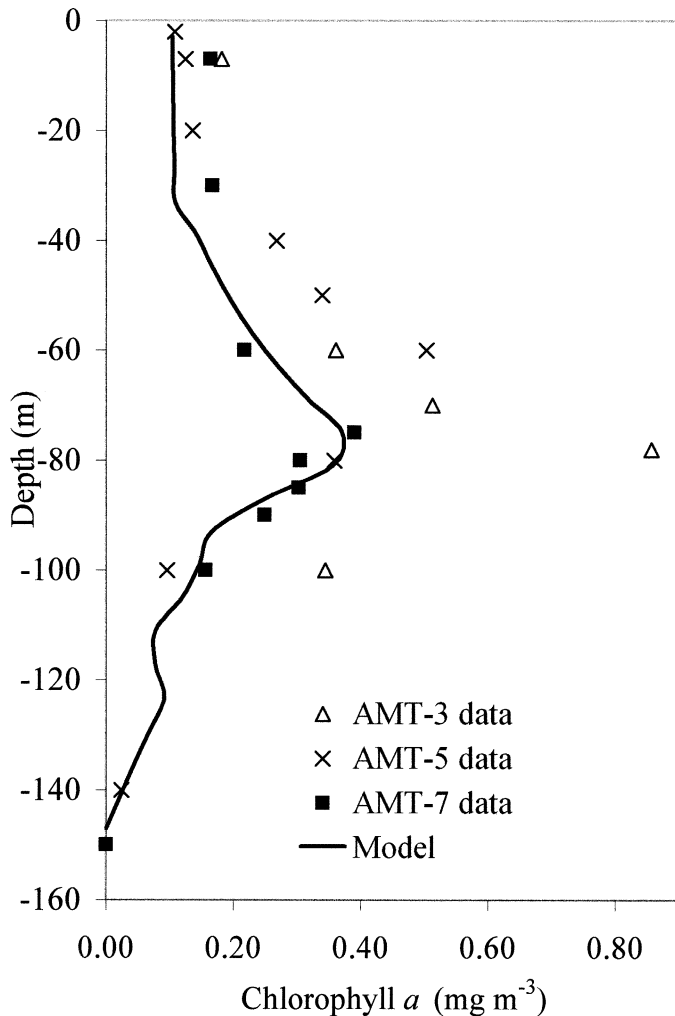


Fig. 1. Modeled Chl *a* profile at day 281 (October) compared with the Atlantic Meridional Transect (AMT) data at 1.29°N, 25.78°W in 1996 (AMT-3), at 0.77°N, 25.66°W in 1997 (AMT-5), and at 0°, 25°W in 1998 (AMT-7). Although observed nitrate concentrations can be as high as 8 $\mu\text{mol L}^{-1}$ at depth, a nitrate concentration of 2 $\mu\text{mol L}^{-1}$ at 150 m was used in the model to take into account the strong stratification at these latitudes, as in Taylor et al. (1997).

$\text{mg Chl } a \text{ m}^{-3}$, consistent with the weak seasonal cycle of surface irradiance used in this simulation. The modeled Chl *a* profile was within the range observed during Atlantic Meridional Transect (AMT; Aiken et al. 2000). The subsurface Chl *a* maximum occurred at a depth of 75 m in the model, in agreement with the October 1998 data (Fig. 1). The predicted Chl *a* was slightly lower than observed in October 1998 but matched the October 1996 data.

Although the modeled Chl *a* profile compared well with the observations, the simulated phytoplankton C:N of 11 g C (g N) $^{-1}$ at the surface was higher than the observations for particulate C:N of 7 for the equatorial Atlantic reported by Bishop et al. (1977). The phytoplankton C:N was over twice the Redfield ratio of 5.7 g C (g N) $^{-1}$ = 6.6 mol C (mol N) $^{-1}$ and was significantly greater than values of 5.9–8.1 obtained from ^{14}C labeling of protein in the subtropical

Pacific Ocean (Laws et al. 1989; Allen et al. 1996) and Caribbean Sea (Taguchi et al. 1988).

Given this mismatch between modeled phytoplankton C:N and observations of particulate C:N described above, we examined the sensitivity of modeled Chl *a* distributions and surface phytoplankton C:N to variations in the values of the physiological parameters (P_{m}^{C} , Q_{min} , and α_{Chl}), the vertical mixing coefficient (k), the mortality (m), and the maximum recycling efficiency (ε_{max}).

Sensitivity to parameterization of phytoplankton physiology: In the standard run, Q_{min} was set at 0.04 g N (g C) $^{-1}$, corresponding to a phytoplankton C:N of 25 g C (g N) $^{-1}$. This value was based on Geider et al. (1998) for cultures grown under continuous illumination and might be an unrealistically high C:N for phytoplankton growing on a light-dark cycle. For example, DiTullio and Laws (1986) found that phytoplankton C:N ranged from 18.7 g C (g N) $^{-1}$ at low nutrient-limited growth rates to 5.7 g C (g N) $^{-1}$ under nutrient-saturated conditions. For the sensitivity analysis, we altered Q_{min} to 0.06 g N (g C) $^{-1}$, corresponding to a maximum phytoplankton C:N of about 16.7 g C (g N) $^{-1}$. Increasing Q_{min} did not significantly affect the Chl *a* distribution (Fig. 2C) and contributed to a moderate decrease of phytoplankton C:N (Table 2).

Reducing $P_{\text{max}}^{\text{C}}$ from 2.0 d $^{-1}$ to 1.5 d $^{-1}$ led to lower surface Chl *a* concentrations (Fig. 2A). In turn, lower surface Chl *a* decreased light attenuation and the deeper penetration of light led to deepening of the subsurface Chl *a* maximum from a peak at 75 m to a peak at 80 m (Fig. 2A). A lower $P_{\text{max}}^{\text{C}}$ was associated with a slight decrease of surface phytoplankton C:N (Table 2), but phytoplankton C:N remained higher than the Redfield ratio and the observed particulate C:N values (Table 2). Increasing $P_{\text{max}}^{\text{C}}$ resulted in higher surface Chl *a* values (Fig. 2A) and an increase in the surface phytoplankton C:N (Table 2) but had less effect on the subsurface Chl *a* maximum.

The value of α_{Chl} had a pronounced effect on the depth and the magnitude of the Chl *a* profile, with a stronger and deeper Chl *a* maximum when α_{Chl} was increased (Fig. 2B). However, the surface Chl *a* remained the same (Fig. 2B), and phytoplankton C:N was only slightly altered compared to the standard run (Table 2).

Over the range of values for Q_{min} , $P_{\text{max}}^{\text{C}}$, and α_{Chl} examined in Fig. 2, the surface phytoplankton C:N varied from 9.8 to 12.5 g C (g N) $^{-1}$, as compared with 11.3 g C (g N) $^{-1}$ in the standard run (Table 2). Declines of surface phytoplankton C:N were associated with increases of Q_{min} , decreases of $P_{\text{max}}^{\text{C}}$, and decreases of α_{Chl} (Table 2).

Sensitivity to parameterization of physical mixing: A change of the physical parameters can affect the phytoplankton by modifying the nutrient supply and thus the Chl *a* distribution. For the prescribed physics, the supply of nutrients was determined by the mixing coefficient, k . Increasing k increased the flux of nutrients to the mixed layer and significantly increased the surface Chl *a* concentration (Fig. 2D). In contrast, lowering k reduced the flux of nutrients to the surface and accentuated the deep Chl *a* maximum layer (Fig. 2D). Although the Chl *a* profile was very sensitive to

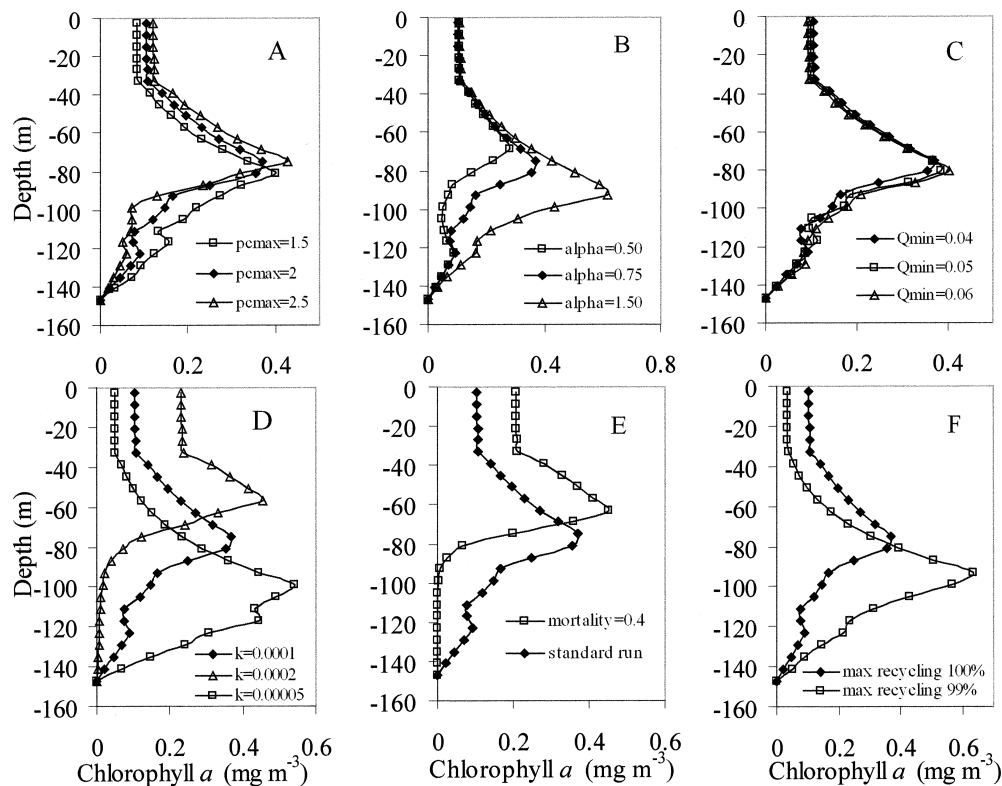


Fig. 2. Modeled Chl *a* profile at the equator at day 281 for different parameter values: (A) the maximum photosynthesis rate P_{\max}^C , (B) the slope of the P-I curve α_{chl} , (C) the upper limit of C:N Q_{\min} , (D) the mixing coefficient k , (E) the parameterization of the mortality, and (F) the maximum recycling efficiency.

the value of the mixing coefficient, the surface value of phytoplankton C:N was only reduced from 11.3 in the standard run to 10.8 when k was doubled (Table 2). The change in k that would be required to significantly lower phytoplankton C:N, would be accompanied by a much higher surface Chl *a* concentration than was observed (Fig. 2).

Sensitivity to parameterization of mortality and nutrient recycling: In a system where most of the phytoplankton production is supported by recycled nutrients, the growth rate of phytoplankton will be closely coupled to the rate of nutrient regeneration. Through the control of growth rate, mortality and recycling are processes that also affect phytoplankton C:N. The standard run assumed a constant mortality of 0.8 d^{-1} in the mixed layer and a linear decrease with depth to a mortality of zero at 120 m. The Chl *a* profile was sig-

nificantly different when a constant mortality of 0.4 d^{-1} was used throughout the water column (Fig. 2E). High mortality at depth shifted the balance of nutrient regeneration toward shallower depths, increasing the nutrient flux to the surface layer. Higher Chl *a* in the surface mixed layer reduced light penetration and, hence, photosynthesis at depth, which together with the increased mortality at depth caused the subsurface Chl *a* maximum to become shallower and slightly more pronounced. This parameterization of mortality strongly affected the surface phytoplankton C:N, which was about 30% higher than with the standard run (Table 3).

High mortality is required in the surface layer to yield a low C:N ratio, but lower mortality is required at depth to obtain a realistic deep Chl *a* maximum. If m is held constant throughout the water column, then either surface C:N will be too high if a low m is chosen or the subsurface Chl *a* maximum will be too shallow if a high m is chosen. Our parameterization of the depth dependence of mortality (m) from 0.8 d^{-1} in the mixed layer to 0 d^{-1} with increasing depth is crucial to obtain correct vertical Chl *a* profiles.

The recycling of nutrients within the mixed layer also affected phytoplankton dynamics. Reducing the maximum value of the recycling efficiency from 100 to 99% resulted in loss of nutrients from the mixed layer and reduction in the surface Chl *a* concentration (Fig. 2F). This allowed deeper light penetration, leading to a stronger and deeper subsurface Chl *a* maximum (Fig. 2F). Despite this significant change of

Table 3. Surface values of phytoplankton carbon to nitrogen (C:N, $\text{g C} [\text{g N}]^{-1}$) and carbon to Chl *a* (C:Chl *a*, $\text{g C} [\text{g Chl } a]^{-1}$) ratios and phytoplankton nitrogen (PhyN, mmol m^{-3}) for loss tests (recycling efficiency, mortality).

	Standard run	$\epsilon_{\max} = 99\%$	Constant mortality of 0.4 d^{-1}
C:N	11.3	11.8	14.5
C:Chl <i>a</i>	95	105	124
PhyN	0.062	0.023	0.126

the Chl *a* distribution, surface phytoplankton C:N remained similar to the standard run (Table 3). Thus, a slight change in the treatment of recycling had a pronounced effect on the Chl *a* profiles.

Summary: The sensitivity analysis described above demonstrates that significant changes in the vertical Chl *a* distribution were not systematically related to the surface phytoplankton C:N. The sensitivity analysis for the equatorial simulation indicated the following.

1. The vertical diffusivity had marked effects on the vertical Chl *a* profile but had little effect on mixed layer phytoplankton C:N.
2. The physiological parameters P_m^C and Q_{min} had moderate effects on Chl *a* profile and surface phytoplankton C:N.
3. The initial slope of the P-I curve, α_{Chl} , markedly affected the vertical Chl *a* profile and had a moderate effect on phytoplankton C:N.
4. The parameterization of mortality had marked effects on both the vertical Chl *a* profile and the mixed layer phytoplankton C:N.

Only two of the runs yielded phytoplankton C:N values as small as 9.8–9.9, and these used either the low P_{max}^C or the high value for Q_{min} . The most significant decrease of phytoplankton C:N was obtained when Q_{min} was increased to 0.06 and P_{max}^C was simultaneously lowered (Table 2), leading to a phytoplankton C:N of 9 g C (g N)⁻¹. Using $P_{max}^C = 1.5 \text{ d}^{-1}$, $Q_{min} = 0.06$, $\alpha_{Chl} = 0.95 \times 10^{-5} \text{ g C m}^2 (\text{g Chl } a \text{ } \mu\text{mol photons})^{-1}$, $k = 0.0002 \text{ m}^2 \text{ s}^{-1}$, and a maximum recycling efficiency of 100% led to a chlorophyll profile in broad agreement with the observations (Fig. 3) and a surface C:N < 9.

Subtropical Atlantic simulation—We used the parameter values that arose from the sensitivity analysis (Fig. 2) conducted at the equator to simulate the seasonal and vertical dynamics of Chl *a*, phytoplankton C:N, phytoplankton C:Chl *a*, primary productivity, and export production for the Bermuda Atlantic Time-series Study (BATS) site, where the seasonal cycles in mixed layer depth and temperature are stronger than at the equator. The mortality in the mixed layer was assumed to follow the seasonal cycle of temperature, as in Taylor et al. (1991), with a minimum winter value of 0.3 d⁻¹ and a maximum summer mortality of 0.8 d⁻¹ (the same as the value used at the equator). As in the standard tropical simulations, the mortality coefficient, m , was assumed to decline linearly with increasing depth between the bottom of the mixed layer and 120 m, where it was set equal to 0.05 d⁻¹. A maximum recycling efficiency of 0.98 was used. All other parameter values are as in Fig. 3.

The model output was compared with observations of Chl *a* concentration (Figs. 4A, 5), primary productivity (Fig. 4B), and vertical particulate nitrogen sinking rates (Fig. 4C) collected at BATS from 1994 to 1998 (obtained from <http://www.bbsr.edu/users/ctd/>), as well as with Goericke and Welschmeyer's (1998) data for phytoplankton C:Chl *a* for 1985–1987 (Figs. 6, 7) and BATS data for particulate C:N (Fig. 8).

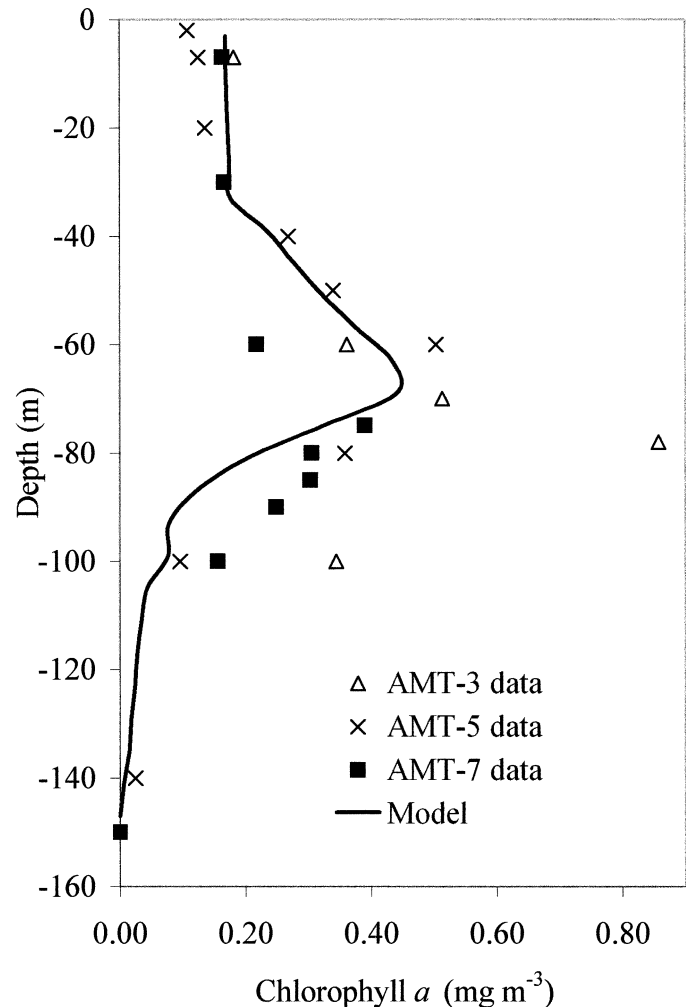


Fig. 3. As in Fig. 1 but with new input parameters for the model run: $P_{max}^C = 1.5 \text{ d}^{-1}$, $Q_{min} = 0.06 \text{ g C (g N)}^{-1}$, and $\alpha_{Chl} = 0.95 \times 10^{-5} \text{ m}^2 (\text{g Chl } a)^{-1}$.

Chl *a* and primary productivity: The model produced a seasonal cycle of surface Chl *a* concentration that was similar in magnitude to the observations but lagged the observed spring bloom by 1–2 months (Fig. 4A). In addition to reproducing the seasonal cycles of surface Chl *a*, the subsurface Chl *a* maximum was well reproduced (Fig. 5), except in January, where the model tended to underestimate the Chl *a* concentrations throughout the water column (Fig. 5A). At other times of the year, the depth and the magnitude of the subsurface Chl *a* maximum were within the range of observations.

The model produced a seasonal cycle of water column integrated net primary productivity that compared well with the observations of light minus dark bottle 24-h ¹⁴C assimilation rates (Fig. 4B). The magnitude of net primary productivity predicted by the model (200–900 mg C m⁻² d⁻¹) fell within the range of the observations (150–950 mg C m⁻² d⁻¹). The model also reproduced the observed midwinter productivity minimum, spring productivity maximum, and slow decline of productivity through summer and autumn that was evident in the observations.

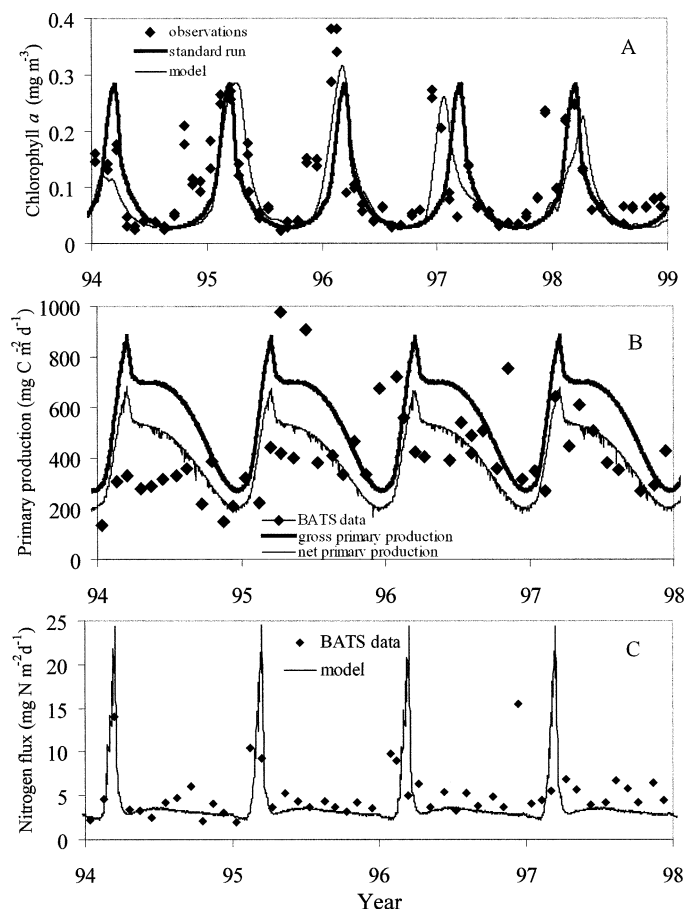


Fig. 4. (A) Modeled seasonal cycle of surface Chl *a* (solid line) compared with observations (0–15 m depth range) at BATS. A run with measured mixed layer depths at BATS is also shown (dashed line). (B) Modeled seasonal cycle of water column gross (upper curve) and net (lower curve) primary productivity (0–140 m) compared with observations of 24-h ¹⁴C light minus dark bottle productivity (0–140 m) at BATS. (C) Modeled seasonal cycle of organic nitrogen export (solid line) compared with observations of particulate nitrogen sinking flux at 150 m at BATS. The model output is compared with observations from January 1994 to December 1998.

Nitrogen export: The model provided estimates of organic nitrogen export that were similar in magnitude to the observed vertical particulate nitrogen fluxes at 150 m throughout most of the annual cycle (Fig. 4C). However, the model produced a sharp spring peak in the organic N export flux of 24 mg N m⁻² d⁻¹ that was about twice the maximum flux observed at BATS in 1997 and 1998 and much larger than the values observed in other years. This peak was associated with a deepening of the mixed layer in March (day 75), allowing nitrate-rich subsurface water into the mixed layer. It also coincided with the Chl *a* peak (Fig. 4A) and high primary productivity (Fig. 4B). Annual modeled primary and export productions are compared with observations at BATS (Table 4).

It is tempting to interpret the general agreement of the model-derived values of nitrogen export with the observations of sinking particulate organic nitrogen fluxes (Fig. 4C)

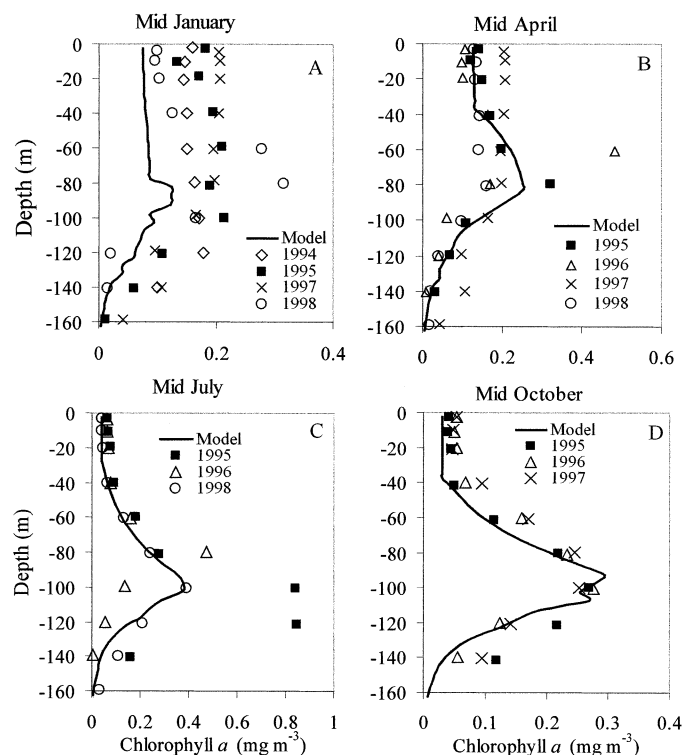


Fig. 5. Modeled Chl *a* profile (solid line) compared with observations at BATS in (A) mid-January, (B) mid-April, (C) mid-July, and (D) mid-October.

as indicating that the prescribed physics, despite its simplicity, yielded the correct flux of nitrate into the euphotic zone. However, this might not be the case, since the observed sediment trap nitrogen flux at BATS of 0.10 ± 0.07 mol N m⁻² yr⁻¹ is only about 20% of the estimated nitrate flux on the basis of deep-water oxygen utilization rates (Siegel et al. 1999). Nitrogen fixation (Gruber and Sarmiento 1997), which is not included in our model, might account for part of the discrepancy. However, it might also be necessary to take horizontal transport, eddy pumping, or both into account (Siegel et al. 1999).

Prescription of additional new nitrogen inputs, such as nitrogen fixation, would require reassessment of our treatment of recycling. Our treatment, with a maximum recycling efficiency of 98%, conserves nitrogen very efficiently at low inorganic nitrogen levels. This high recycling efficiency would need to be relaxed if additional sources of new nitrogen were included in the model in order to achieve seasonal cycles of Chl *a* and primary productivity that are consistent with observations. Increasing nitrogen inputs would also lead to a mismatch between our modeled nitrogen export and the measured sediment trap fluxes.

Comparison with forcing by observed mixed layer depth: One of the major mismatches between the model and the observations lies in the timing of the spring bloom, which occurs earlier in reality than in the simulation. This could be because of our use of a climatology of mixed layer depth that does not accurately reflect interannual variability of mixed layer dynamics. When forced with the climatology of

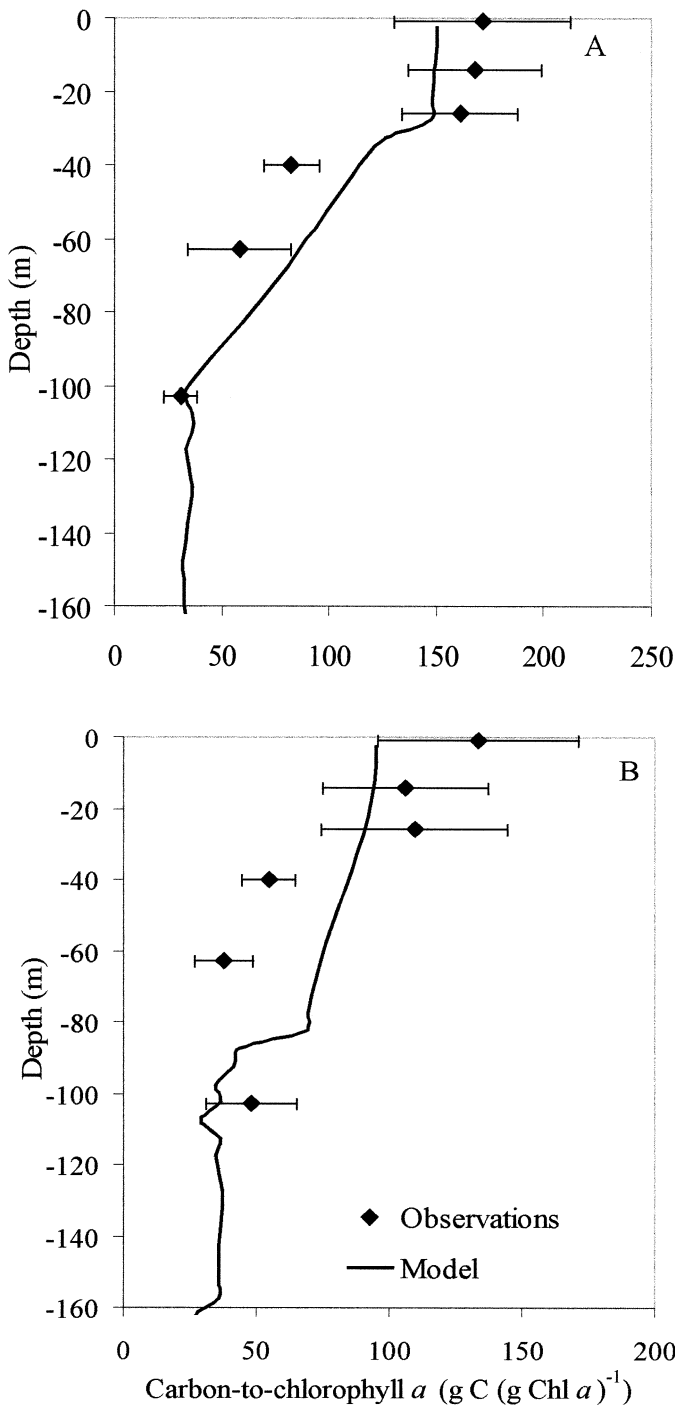


Fig. 6. Modeled vertical profiles of phytoplankton C:Chl *a* compared with observations of Goericke and Welschmeyer (1988) for (A) summer and (B) winter. Goericke and Welschmeyer's data, originally reported as a function of optical depth, were converted to absolute depth using a light attenuation coefficient of 0.04016 m^{-1} . Shown are the mean \pm SD of the observations and the model profiles for days 90 (winter) and 925 (summer).

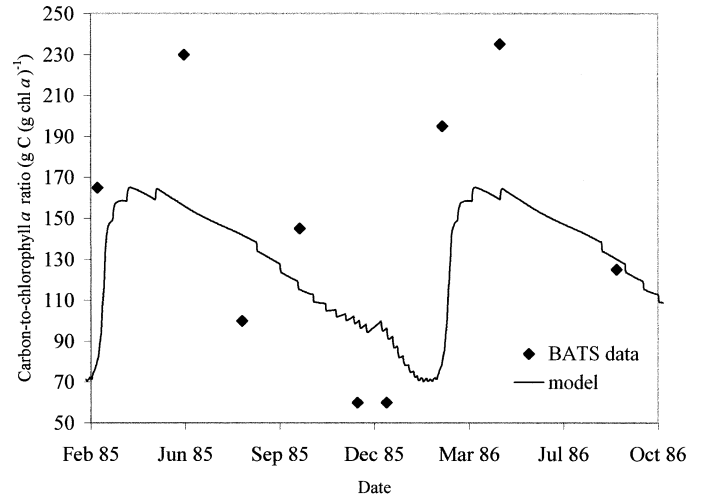


Fig. 7. Modeled seasonal cycle of C:Chl *a* compared with observations of Goericke and Welschmeyer (1988) at BATS.

mixed layer depth, the model accounted for 29% of the variance ($r^2 = 0.29$) in mixed layer Chl *a* concentrations. The mixed layer depth at BATS was calculated from temperature and salinity profiles as that depth at which the difference in density was $>0.125 \text{ kg m}^{-3}$. Forcing the model with the observed mixed layer depths (with a mixed layer diffusivity

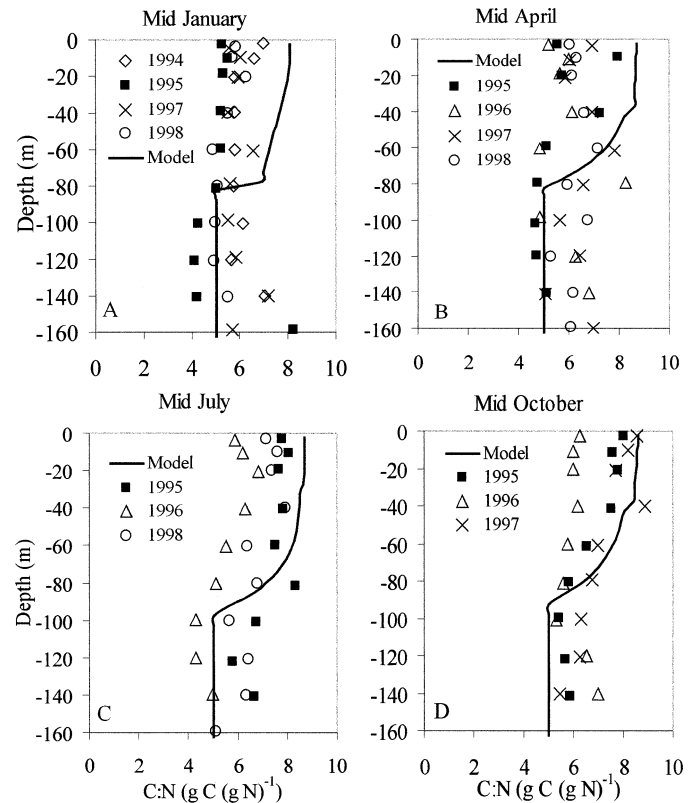


Fig. 8. Modeled vertical profiles of phytoplankton C:N (solid line) compared with the particulate organic carbon to particulate organic nitrogen ratio at BATS in (A) mid-January, (B) mid-April, (C) mid-July, and (D) mid-October.

Table 4. Annual means of gross production, net production ($\text{mg C m}^{-2} \text{d}^{-1}$) and particulate nitrogen export ($\text{mg N m}^{-2} \text{d}^{-1}$) for the run with climatological mixed layer, the run with observed mixed layer depth, and the observations from BATS.

Year	Gross primary production model	Net primary production		Nitrogen export	
		Model	Observations	Model	Observations
Climatology	548	401	—	4.02	—
1994–1995	511	367	275	3.62	4.44
1995–1996	650	492	484	7.86	4.82
1996–1997	646	485	491	6.99	6.31
1997–1998	563	416	414	4.54	5.21
1998–1999	587	442	328	5.98	4.98
Mean ($n = 5$)		440	398	5.80	5.15
SD		52	95	1.73	0.71

coefficient of $0.0015 \text{ m}^2 \text{ s}^{-1}$) at BATS reduced, but did not eliminate, the mismatch in the timing of the spring bloom and increased the proportion of variance explained by the model to 42% (Fig. 4A). It might be unrealistic to expect a one-dimensional model to explain more of the variance in the observations at BATS given the role of horizontal transport in this region. For example, Fasham et al. (1993), using a three-dimensional model, showed that horizontal advection accounted for a greater proportion of the nitrogen flux at BATS ($398 \text{ mmol N m}^{-2} \text{ yr}^{-1}$) than did vertical convection ($343 \text{ mmol N m}^{-2} \text{ yr}^{-1}$).

The mixed layer diffusion coefficient had to be reduced to avoid severely overestimating the magnitude of the spring bloom Chl *a*, primary productivity, and export production (data not shown) when the observed mixed layer depths were used. To obtain better agreement between the model and data might require forcing of both mixed layer depth and vertical diffusivity; however, this is beyond the scope of our research. Using the observed mixed layer depths in conjunction with a fixed, but reduced, value of the diffusivity led to good agreement ($r^2 = 0.66$ for $n = 5$) between model output and observed interannual variability in annual average daily net primary productivity (Table 4). In contrast, the model output accounted for only a small proportion ($r^2 = 0.19$) of the observed interannual variability in average export production (Table 4).

Phytoplankton C:Chl *a*: The modeled phytoplankton C:Chl *a* profiles were compared to the observations of Goericke and Welschmeyer (1998) (Fig. 6). Similar values of about $30 \text{ g C (g Chl } a)^{-1}$ were obtained at a depth of 100 m in both summer and winter. Surface values of $150 \text{ g C (g Chl } a)^{-1}$ in summer and $100 \text{ g C (g Chl } a)^{-1}$ in winter obtained from the model were slightly lower than the mean values observed by Goericke and Welschmeyer (1998) but fell within ± 1 SD of the measurements (Fig. 6). That the observations show a more rapid decline from surface to subsurface values of C:Chl *a* than the model might indicate a limitation of static (fixed depth) incubations in which some degree of photoacclimation might occur during the incubation. The seasonal cycle of surface phytoplankton C:Chl *a* from 70 to $170 \text{ g C (g Chl } a)^{-1}$ predicted by the model (Fig. 7) follows the same pattern as the observations, although the observed values vary more widely.

Phytoplankton C:N: The simulated surface phytoplankton C:N, with a maximum value in summer around 9 g C (g N)^{-1} , was slightly higher than the particulate organic C:N at BATS, which is typically 8 g C (g N)^{-1} in summer (Fig. 8). The agreement with the observations was better below 60 m (Fig. 8). Unlike the model, which shows a vertical gradient of phytoplankton C:N, the observations of particulate C:N do not show a depth dependence.

The values of phytoplankton C:N that our model generates are consistent with the upper range of particulate C:N observed in oligotrophic ocean regions. However, particulate C:N does not necessarily correspond to the phytoplankton C:N because the living component of particulate matter includes bacteria and phagotrophic protists, which have lower C:N than phytoplankton. Phytoplankton account for about 50% of the living biomass in the $<20\text{-}\mu\text{m}$ size range in the open ocean, with bacteria accounting for most of the rest (Campbell et al. 1994; Buck et al. 1996). If heterotrophic bacteria have a C:N of 4 g g^{-1} (Nagata 1986; Fagerbakke et al. 1996), and the biomass can be divided equally between phytoplankton and heterotrophic bacteria, then the C:N for bulk particulate matter of $6\text{--}8 \text{ g C (g N)}^{-1}$ implies a phytoplankton C:N of $8\text{--}10 \text{ g C (g N)}^{-1}$. These values are within the range of phytoplankton C:N generated by the model. However, this calculation, based on particulate C:N and the partitioning of C and N between bacterioplankton and phytoplankton, neglects detritus, which could account for 25–50% (Campbell et al. 1994; Claustre et al. 1999) of particulate organic matter.

A more direct assessment of phytoplankton C:N is provided by the proportion of ^{14}C that is incorporated into protein during 24-h (dawn to dawn) productivity measurements (Ditullio and Laws 1986). Laws et al. (1989) and Allen et al. (1996) calculated phytoplankton C:N values of $5.9\text{--}8.1 \text{ g C (g N)}^{-1}$ for the phytoplankton of the North Pacific Central Gyre. In contrast, Smith and D'Souza (1993) found that the proportion of ^{14}C assimilated into protein varied with irradiance in the oligotrophic waters of the North Atlantic ($37^\circ\text{N } 41^\circ\text{W}$) in April 1990. Our calculations of phytoplankton C:N based on Smith and D'Souza's data yield values of 6 g C (g N)^{-1} at the 2% light level and $10\text{--}11.5 \text{ g C (g N)}^{-1}$ at the 22 and 90% light levels. These observations exceed the values obtained in the simulations. Smith and D'Souza's (1993) observations were made at the end of the spring

bloom before the microbial loop would have become well established and when nutrient stress would be expected to be particularly severe and might not apply later in the season.

Phytoplankton growth rate in situ: Phytoplankton growth rate provides an additional variable that can be used to evaluate model performance. Growth rates in the mixed layer of oligotrophic gyres are reported to be about 0.6 to 0.7 d⁻¹ based on diel variations in phytoplankton abundance and dilution-grazing experiments (Lessard and Murrell 1998; Claustre et al. 1999; Stelfox-Widdicombe et al. 2000). The reported rates for Sargasso Sea phytoplankton assemblages are somewhat lower than the maximum growth rate of an oligotrophic ocean isolate of *Synechococcus* of 2.0 d⁻¹ at 26°C (Kana and Glibert 1987) and the iron-replete growth rate of 1.4 d⁻¹ for *Prochlorococcus* in the equatorial Pacific Ocean (Mann and Chisholm 2000). This difference in rates is consistent with the nutrient limitation of phytoplankton growth rate, as inferred from the model.

Our model yields phytoplankton growth rates for the mixed layer at the BATS site that range from 0.9 d⁻¹ in summer to 0.5 d⁻¹ during the peak of the spring bloom. Many models of phytoplankton dynamics in the upper ocean can achieve realistic simulations of seasonal cycles of Chl *a* and nutrient fields but fail to obtain estimates of phytoplankton growth rates that are consistent with observations. Earlier models for Bermuda returned growth rates that were three to four times lower. For example, the Fasham et al. (1990) model, which provides a basic structure that has been the starting point for many other recent models, yields phytoplankton growth rates in the mixed layer at Bermuda in summer of about 0.2 d⁻¹. Other models for Bermuda mixed layer in summer yield phytoplankton growth rates of 0.1–0.2 d⁻¹ (Doney et al. 1996). An exception is the model of Hurtt and Armstrong (1996), which yielded a phytoplankton growth rate of about 1 d⁻¹. However, this model was formulated such that the maximum growth rates for irradiance-limited and nitrogen-limited growth were allowed to differ significantly, being about 3 d⁻¹ for light and 1 d⁻¹ for inorganic nitrogen. A more recent model of Hurtt and Armstrong (1999) yielded $\mu < 0.1$ d⁻¹. The recent model of Moore et al. (2001), which used the same treatment of phytoplankton physiology as we employed in this paper, yielded the same range of growth rates as our model (0.3 d⁻¹ in winter to 0.7 d⁻¹ in summer) when applied to BATS. Thus, it appears that a physiological model can yield realistic estimates of phytoplankton growth and relative growth rates. However, as noted previously in the sensitivity analysis for the equatorial simulation, the parameterization of phytoplankton mortality (*m*) was critical in achieving high relative growth rates and realistic vertical Chl *a* profiles.

We have shown that a physiological model of phytoplankton growth, when embedded within a simple model of physical mixing, mortality, and recycling can simulate the seasonal and vertical distributions of biomass, primary productivity, phytoplankton C:Chl *a* and C:N ratios. The simplicity of our model structure, which includes only phytoplankton and inorganic nitrogen as state variables, is perhaps deceptive. The prescribed seasonal and depth-depen-

dent mortality in our model is essential for successful model performance. This prescription shows the essential features of phytoplankton mortality that are required of a model to fit the BATS data. Although prescribed, the depth dependence of mortality is consistent with observations (Liu et al. 1997), and the seasonal dependence is based on the assumption that mortality, like other biological rate constants, increases with increased temperature. Also essential to successful model performance is the parameterization of nutrient recycling efficiency as a function of inorganic nitrogen concentration. This parameterization is not unlike that employed by Platt and Harrison (1985) on the basis of observations of the nutrient dependence of the *f*-ratio. However, it was necessary for us to set a very high maximum recycling efficiency of 98% in order to obtain a realistic simulation at BATS. It is likely that this high recycling efficiency compensates for incomplete accounting of the sources of new nitrogen to the euphotic zone in our model.

Despite the limitations of our treatment of physical mixing, mortality, and recycling, the model produces convincing simulations of annual cycles of Chl *a* concentration and primary productivity. That the model produces simulations of phytoplankton C:Chl *a* that compare favorably with the most extensive data set available for oligotrophic ocean phytoplankton and yields estimates of phytoplankton C:N that are consistent with the limited observations that are available suggests that the Geider et al. (1998) dynamic model of phytoplankton growth and acclimation can provide a link between bio-optics, nitrogen cycling, and carbon cycling.

References

- AIKEN, J., AND OTHERS. 2000. The Atlantic Meridional Transect: Overview and synthesis of data. *Prog. Oceanogr.* **45**: 257–312.
- ALLEN, C. B., J. E. KANDA, AND A. LAWS. 1996. New production and photosynthetic rates within and outside a cyclonic meso-scale eddy in the North Pacific Subtropical Gyre. *Deep-Sea Res.* **43**: 917–936.
- BISHOP, J. K. B., J. M. EDMOND, D. R. KETTER, M. P. BACON, AND W. B. SILKER. 1977. The chemistry, biology and vertical flux of particulate matter from the upper 400 m of the equatorial Atlantic Ocean. *Deep-Sea Res. I* **24**: 511–548.
- BUCK, K. R., F. P. CHAVEZ, AND L. CAMPBELL. 1996. Basin-wide distributions of living carbon components and the inverted trophic pyramid of the central gyre of the North Atlantic Ocean, summer 1993. *Aquat. Microb. Ecol.* **10**: 283–298.
- CAMPBELL, L., H. A. NOLLA, AND D. VAULOT. 1994. The importance of *Prochlorococcus* to community structure in the central North Pacific Ocean. *Limnol. Oceanogr.* **39**: 954.
- CLAUSTRE, H., AND OTHERS. 1999. Variability in particle attenuation and chlorophyll fluorescence in the tropical Pacific: Scales, patterns, and biogeochemical implications. *J. Geophys. Res.* **104**: 3401–3422.
- DiTULLIO, G. R., AND E. A. LAWS. 1986. Diel periodicity of nitrogen and carbon assimilation in five species of marine phytoplankton: Accuracy of methodology for predicting N-assimilation rates and N/C composition ratios. *Mar. Ecol. Prog. Ser.* **32**: 123–132.
- DONEY, S. C., D. M. GLOVER, AND R. G. NAJJAR. 1996. A new coupled, one-dimensional biological-physical model for the upper ocean: Applications to the JGOFS Bermuda Atlantic Time-series Study (BATS) site. *Deep-Sea Res.* **43**: 591–624.
- FAGERBAKKE, K. M., M. HELDAL, AND S. NORLAND. 1996. Content

- of carbon, nitrogen, oxygen, sulfur and phosphorus in native aquatic and cultured bacteria. *Aquat. Microb. Ecol.* **10**: 15–27.
- FASHAM, M. J. R., H. W. DUCKLOW, AND S. M. MCKELVIE. 1990. A nitrogen-based model of plankton dynamics in the oceanic mixed layer. *J. Mar. Res.* **48**: 591–639.
- , J. L. SARMIENTO, R. D. SLATER, H. W. DUCKLOW, AND R. G. WILLIAMS. 1993. Ecosystem behavior at Bermuda Station “S” and Ocean Weather Station “India”: A general circulation and observational analysis. *Glob. Biogeochem. Cycles* **7**: 379–415.
- GEIDER, R. J., H. L. MACINTYRE, AND T. M. KANA. 1998. A dynamic regulatory model of phytoplankton acclimation to light, nutrients, and temperature. *Limnol. Oceanogr.* **43**: 679–694.
- GOERICKE, R., AND N. A. WELSCHMEYER. 1998. Response of Sargasso Sea phytoplankton biomass, growth rates and primary production to seasonally varying physical forcing. *J. Plankton Res.* **20**: 2223–2250.
- GRUBER, N., AND J. L. SARMIENTO. 1997. Global patterns of marine nitrogen fixation and denitrification. *Glob. Biogeochem. Cycles* **11**: 235–266.
- HURTT, G. C., AND R. A. ARMSTRONG. 1996. A pelagic ecosystem model calibrated with BATS data. *Deep-Sea Res. II* **43**: 653–683.
- , AND ———. 1999. A pelagic ecosystem model calibrated with BATS and OWSI data. *Deep-Sea Res.* **46**: 27–62.
- KANA, T. M., AND P. M. GLIBERT. 1987. Effect of irradiances up to 2000 $\mu\text{E m}^{-2} \text{s}^{-1}$ on marine *Synechococcus* wh7803 1. Growth, pigmentation and cell composition. *Deep-Sea Res.* **34**: 479–495.
- LAWS, E. A., G. R. DiTULLIO, P. B. BETZER, D. M. KARL, AND K. L. CARDER. 1989. Autotrophic production and elemental fluxes at 26°N, 155°W in the North Pacific Subtropical Gyre. *Deep-Sea Res.* **36**: 130–120.
- LESSARD, E. J., AND M. C. MURRELL. 1998. Microzooplankton herbivory and phytoplankton growth in the northwestern Sargasso Sea. *Aquat. Microb. Ecol.* **16**: 173–188.
- LEVITUS, S., AND T. BOYER. 1994. World Ocean Atlas 1994 Volume 4: Temperature. U.S. Department of Commerce.
- LIU, H., H. A. NOLLA, AND L. CAMPBELL. 1997. *Prochlorococcus* growth rate and contribution to primary production in the equatorial and subtropical North Pacific Ocean. *Aquat. Microb. Ecol.* **12**: 39–47.
- MANN, E. L., AND S. W. CHISHOLM. 2000. Iron limits the cell division rate of *Prochlorococcus* in the eastern equatorial Pacific. *Limnol. Oceanogr.* **45**: 1067–1076.
- MOORE, J. K., S. C. DONEY, J. A. KLEYPAS, D. M. GLOVER, AND I. Y. FUNG. 2001. An intermediate complexity marine ecosystem model for the global domain. *Deep-Sea Res.* **49**: 403–462.
- MOREL, A. 1988. Optical modeling of the upper ocean in relation to its biogenous matter content (case I waters). *J. Geophys. Res.* **93**: 10,749–10,768.
- NAGATA, T. 1986. Carbon and nitrogen content of natural planktonic bacteria. *Appl. Environ. Microbiol.* **52**: 28–32.
- PLATT, T., AND W. G. HARRISON. 1985. Biogenic fluxes of carbon and oxygen in the ocean. *Nature* **318**: 55–58.
- SARMIENTO, J. L., M. J. R. FASHAM, U. SIEGENTHALER, R. G. NAJJAR, AND J. R. TOGGWEILER. 1989. Models of chemical cycling in the ocean: Progress report II. Princeton Univ.
- SELLERS, W. D. 1965. Physical climatology. Univ. of Chicago Press.
- SIEGEL, D. A., D. J. MCGILLICUDDY, AND E. A. FIELDS. 1999. Mesoscale eddies, satellite altimetry, and new production in the Sargasso Sea. *J. Geophys. Res.* **104**: 13,359–13,380.
- SMITH, R. E. H., AND F. M. L. D’SOUZA. 1993. Macromolecular labelling patterns and inorganic nutrient limitation of a North Atlantic spring bloom. *Mar. Ecol. Prog. Ser.* **92**: 111.
- STELFOX-WIDDICOMBE, C. E., E. S. EDWARDS, P. H. BURKILL, AND M. A. SLEIGH. 2000. Microzooplankton grazing activity in the temperate and sub-tropical NE Atlantic: Summer 1996. *Mar. Ecol. Prog. Ser.* **208**: 1–12.
- TAGUCHI, S., G. R. DiTULLIO, AND E. A. LAWS. 1988. Physiological characteristics and production of mixed layer and chlorophyll maximum phytoplankton populations in the Caribbean Sea and western Atlantic Ocean. *Deep-Sea Res.* **35**: 1363–1377.
- TAYLOR, A. H., A. J. WATSON, M. AINSWORTH, J. E. ROBERTSON, AND D. R. TURNER. 1991. A modelling investigation of the role of phytoplankton in the balance of carbon at the surface of the North Atlantic. *Glob. Biogeochem. Cycles* **5**: 151–171.
- , R. J. GEIDER, AND F. J. H. GILBERT. 1997. Seasonal and latitudinal dependencies of phytoplankton carbon-to-chlorophyll *a* ratios: Results of a modelling study. *Mar. Ecol. Prog. Ser.* **152**: 51–66.

Received: 30 July 2002

Accepted: 15 April 2003

Amended: 7 May 2003